Data-Driven Multi-Resolution Probabilistic Energy and Reserve Bidding of Wind Power

Seyyed Ahmad Hosseini, *Student Member, IEEE*, Jean-François Toubeau, *Member, IEEE*, Zacharie De Grève, *Member, IEEE*, Yi Wang, *Member, IEEE*, Nima Amjady, *Senior Member, IEEE*, and François Vallée, *Member, IEEE*

***Abstract*—The current wind farm control schemes qualify wind power producers (WPPs) to provide balancing services in complement to energy in modern electricity markets. Accordingly, WPPs are responsible for real-time deviations in both energy and reserve market floors, which are settled at different time scales. WPPs should adjust their output to cope with fast wind variations, which are critical in the balancing stage. In this paper, we devise a reliable high-temporal-resolution day-ahead bidding framework for WPPs considering the ultra-short-term wind stochasticity. To that end, the model for the bidding strategy is enriched with a probabilistic constraint controlling the confidence level on reserve bids to enhance the reliability of the offered capacity. Additionally, an original Auxiliary Classifier Wasserstein Generative Adversarial Network (ACWGAN) is proposed to generate high-temporal-resolution wind speed scenarios to be embedded into the bidding framework. The numerical results firstly confirm the superiority of the proposed ACWGAN over the other GAN-based alternatives. For instance, ACWGAN can reach 30% higher classification accuracy compared to conditional Wasserstein GAN. Then, the effectiveness of the proposed data-driven method over its single-resolution counterpart and other scenario representation methods is verified regarding the minimization of the negative impact of wind variability on WPPs' profit and reliability of offered reserve bids.**

***Index Terms*—Wind power, probabilistic bidding, balancing service, Auxiliary Classifier Wasserstein GAN, multi-resolution uncertainty.**

NOMENCLATURE

A. Sets and Indices

T/t	Market time intervals.
Ω/ω	Scenarios of hourly mean wind power.
Δ/δ	Balancing periods in each market interval.
V/ν	Scenarios of minute-wise wind deviations.
X and Ψ	Sets of first- and second-stage variables.

B. Decision Variables of the Optimization Framework

$\mathcal{R}$	Revenue of a WPP in the DERM.
P_t^{Eo}/P_t^{Ro}	Day-ahead energy/reserve market power bid at *t*.
$\Delta p_{\omega,t}^{E\uparrow}/\Delta p_{\omega,t}^{E\downarrow}$	Generation surplus/deficit regarding ω and t.
$\Delta p_{\omega,(\nu,\delta),t}^{R}$	Scarcity of reserve capacity for (ν,δ) at ω and *t*.
$z_{\omega,(\nu,\delta),t}$	Binary variable for reserve control strategy.
$p_{\omega,(\nu,\delta),t}^{R}$	Reserve power at *t* regarding ω and (ν,δ).
$p_{\omega,t}^{E}$	Allocated power to energy market at *t* w.r.t ω.
r_t	Risk of reserve unavailability at *t*.

C. Parameters of the Optimization Framework

$\pi_{\omega,t}$	Probability of scenario ω at *t*.
$\mu_{\omega,\nu,t}$	Probability of scenario ν regarding ω at *t*
$\lambda_t^{Eo}/\lambda_t^{Ro}$	Day-ahead energy/reserve price at *t*.
$\lambda_t^{\uparrow}/\lambda_t^{\downarrow}$	Energy imbalance price for $\Delta p_{\omega,t}^{E\uparrow}/\Delta p_{\omega,t}^{E\downarrow}$.
λ_t^{R}	Reserve unavailability penalty at *t*.
$\bar{P}/\underline{P}$	Upper/lower capacity limits of the wind turbine.
$\tilde{P}_{\omega,(\nu,\delta),t}$	Available power at *t* regarding ω and (ν,δ).
$\widetilde{\bar{P}}_{\omega,t}$	Available hourly power at *t* regarding ω.
ρ_t^o	Reserve market participation requirement at *t*.

D. Symbols Used in Scenario Generation Model

$\tilde{w}_t$	Wind speed time-trajectory at *t*
$\bar{w}_t$	Hourly mean value of $\tilde{w}_t$.
ε_t	Ultra-short-term mean deviations w.r.t $\tilde{w}_t$.
$G_\alpha(.)$	Generator with parameters α.
$D_\beta(.)$	Discriminator or critic with parameters β.
$\mathcal{P}_\mathcal{Z}/\mathcal{Z}$	Distribution of latent space/ latent noise vector.
$\mathcal{P}_r/s_r$	Real data distribution / real samples.
$\mathcal{P}_g/s_g$	Generated data distribution/ generated samples.
$\mathcal{L}_W(D_\beta, G_\alpha)$	min-max loss function in WGAN.

Manuscript received 17 May 2021; revised 21 September 2021 and 4 January 2022; accepted 19 February 2022. Date of publication 3 March 2022; date of current version 22 December 2022. This work was supported by the FPS economy, S.M.E.s, Self-employed and Energy through the energy transition funds project BEOWIND. Paper no. TPWRS-00768-2021. *(Corresponding author: Seyyed Ahmad Hosseini.)*

Seyyed Ahmad Hosseini, Jean-François Toubeau, Zacharie De Grève, and François Vallée are with the Electrical Power Engineering Unit, University of Mons, 7000 Mons, Belgium (e-mail: seyyedahmad.hosseiniqarehtapeh@umons.ac.be; jean-francois.toubeau@umons.ac.be; zacharie.degreve@umons.ac.be; francois.vallee@umons.ac.be).

Yi Wang is with the Department of Electrical and Electronic Engineering, The University of Hong Kong, Hong Kong, China (e-mail: yiwang@eee.hku.hk).

Nima Amjady is with the Department of Electrical and Computer Engineering, Semnan University, Semnan 35195-363, Iran (e-mail: amjady@semnan.ac.ir).

Color versions of one or more figures in this article are available at https://doi.org/10.1109/TPWRS.2022.3155865.

Digital Object Identifier 10.1109/TPWRS.2022.3155865

η_{GP}	Gradient penalty coefficient.
$\hat{s}$	Linearly interpolated data points.
θ	Sample taken from uniform distribution U[0, 1]
$\mathcal{P}_c/c$	Class labels distribution / Class label samples.
$\mathcal{L}_{CW}(D_\beta, G_\alpha)$	min-max loss function of CWGAN.
$\mathcal{C}_\varsigma()$	Classifier with parameters ς.
$\mathcal{L}_{AW}(G_\alpha, \mathcal{C}_\varsigma, D_\beta)$	min-min-max loss function of ACWGAN.
$\log \mathbb{P}()$	Log-likelihood loss.
η_c	Hyperparameter of the weight of $\log \mathbb{P}()$.
H_h	Shared layers of ACWGAN with parameters *h*.
$\mathcal{L}^D_{AW}/\mathcal{L}^G_{AW}$	Critic's/ generator's loss function of ACWGAN.

E. Symbols Used in Performance Evaluation

$WD(\mathcal{P}_r, \mathcal{P}_g)$	Wasserstein distance between $\mathcal{P}_r$ and $\mathcal{P}_g$.
γ	Joint distribution with marginals $\mathcal{P}_r$ and $\mathcal{P}_g$.
Γ	Set of all joint distributions of γ.
RMSE $[f, \hat{f}]$	Root mean square error between f and $\hat{f}$.
$d_{i,j}/\tilde{d}_l$	Local alignment cost encoded by *i* and *j* / *l*.
$W = w_1, \ldots, w_L$	Warping path with sequence of *L* pairs.
DTW$[f, \hat{f}]$	Dynamic time warping distance of f and $\hat{f}$.
$\overline{\Delta\mathcal{R}}\%$	Normalized total profit deviation
$\overline{\Delta r}\%$	Risk of reserve unavailability deviation.

I. Introduction

THE growing share of renewable energy resources is a great concern for power system operators that have to continuously accommodate the resulting intermittent and uncertain power supply while ensuring system stability and security [1]. Electricity market policies are therefore emerging for integrating such resources, which is mainly reflected by the advent of spot energy markets and the development of efficient balancing mechanisms (by which system operators can use the flexibility of market actors to maintain a stable system operation). These market opportunities are further complemented with penalty mechanisms whereby deviations between scheduled bids and real-time delivery are charged with an imbalance fee [2]. In this way, the real-time deviations of energy and reserve bids are financially penalized through energy imbalance settlement and balancing stage mechanisms [3]. To reduce the deviation penalties of a wind power producer (WPP) in the day-ahead energy market, a stochastic wind power bidding model is proposed in [4]. In [5], a wind speed forecast is used to identify an optimal wind power bidding profile by minimizing the energy imbalance penalty.

Beyond the participation of WPPs in the energy markets, the current power electronics-based control schemes of wind turbines (WTs) allow them to modulate their available power and offer flexibility to the system [6], [7]. In [8], a day-ahead energy and reserve market (DERM) framework is introduced to motivate WPPs to participate in both energy and reserve market floors. However, in [8], the reserve power deviation penalty at the balancing stage is assumed to be relatively low, so that the WPP is encouraged to submit a riskier reserve bid to the market to make a further profit. In [9], an analytical approach considering hourly wind speed uncertainty and WT control technology is presented to assess the added revenue of WPPs taking part in the DERM. A stochastic bidding framework, considering real-time deviation penalties regarding day-ahead energy and reserve bids, is developed in [10] to maximize WPPs profit in the DERM. The impact of incorporating better hourly forecast information, close to the real-time stage, on WPPs optimal bids is also studied. Overall, in these works, intra-hour wind variability is mostly diverted to the reserve market [8], and thus the offered reserve capacity may not hold high reliability. To circumvent this problem, a stochastic chance-constrained method for wind power scheduling is proposed in [11], where WPP integrates a confidence level on the real-time reserve power delivery as a probabilistic constraint in the bidding framework.

The real-time financial compensation for reserve occurs at a much shorter time interval than the financial compensation for energy deviations in the imbalance settlement mechanism, e.g., minute-wise versus hour-wise [11], [12]. However, all models mentioned above neglect this fact. In particular, due to the difficulty of ultra-short-term wind forecast, the mentioned studies, i.e., [8]–[12], have merely employed hourly wind uncertainty for the remuneration of real-time energy and reserve deviation. This strong assumption may incur opportunity losses due to the poor representation of the wind speed dynamics [12]. More importantly, when ultra-short-term wind variations are high, there is a high risk that the scheduled reserves cannot be deployed in real-time, thus exposing the WPPs to high financial penalties.

In light of this context, there is an increasing need to properly represent the quick dynamics of the wind power behavior and feed this information in dedicated decision tools. Several model-based scenario generation approaches such as copula and auto-regressive moving average are presented in the literature to characterize wind uncertainty [13]. However, the quality of the generated scenarios in such approaches is highly limited by modeling and statistical assumptions [13], [14]. For example, the quality of the scenarios generated via the copula method is extremely sensitive to the copula function chosen to capture the dependence features [15]. As an interesting case, evidence suggests that the 2008 housing crisis in the US was partly due to a misspecified copula function [15]. Additionally, the use of copula in higher dimensions is challenging [16], as it is inflexible in defining multiple dependency structures among features [16]. Therefore, generating ultra-short-term wind scenarios using copula is extremely challenging as each intra-period time step appears as a new dimension.

The recent advancements in generative adversarial networks (GANs) draw wide attention to their application regarding model-free scenario generation for renewable energy sources [13], [14], [17], [18]. The term "model-free" refers to methods that are independent of any prior assumptions about the data distribution [13], [14]. These models can return efficient scenarios by directly learning the diversity and stochasticity of the historical data [14]. In [14], it is shown that conditional GAN

(CGAN) can produce higher quality photovoltaic scenarios in comparison with model-based methods such as copula and Auto-regression. In [13], the Wasserstein GAN (WGAN) model, which has higher training stability compared to GAN, is utilized to produce scenarios for wind and solar power variations with hourly and 5-min temporal resolutions. It is also shown that WGAN produces more effective scenarios compared to the copula method. Additionally, the Lipschitz continuity constraint of Wasserstein distance is imposed by the weight clipping method. In [17], an improved technique to enforce Lipschitz continuity constraint based on gradient penalty is employed in conditional WGAN (CWGAN) to improve the training process. In [18], CWGAN is used to model load forecast uncertainty based on temperature, historical load measurements, and calendar information. However, the performance of CWGAN can be further improved by exploiting an auxiliary classifier (ACWGAN) in the network design to predict the class labels instead of feeding them as an input to the network. It is shown in [19], [20] that such a design can return high-quality outputs for the classification problem of wireless signals. This advanced architecture will be used and optimized in this paper to generate representative forecast scenarios of wind generation with high temporal granularity, which requires advanced adaptation based on wind power expertise.

Importantly, employing the generated wind speed scenarios, via ACWGAN, in the WPP bidding framework is not straightforward since the bidding framework requires wind scenarios in the form of electrical power. Nevertheless, the transformation of wind speed to wind power is a cumbersome task due to the nonlinearities involved in the transfer functions of wind power generators [21]. It is shown that modeling techniques based on the interpolation of manufacturer data reflect the dynamics of WTs better than the ones based on the theoretical cubic relationship between wind speed and power [22]. In this regard, several regression methods such as polynomial, weighted polynomial, cubic B-spline, and penalized cubic B-spline are proposed in the literature [23]. It is shown in [23] that penalized cubic B-spline method, as employed in this paper, better controls the curvature of the fitted power curve.

Overall, this work aims to implement a reliable framework that incorporates the ultra-short-term wind variations into the day-ahead bidding strategy of WPPs in a DERM. The contributions of the paper are three-fold:

1) A novel multi-resolution probabilistic bidding framework is proposed to optimize the profit of WPPs in DERM. Compared with existing works, the minute-level wind power variations are also embedded in the proposed WPP bidding strategy for the first time to precisely model the scheduled reserve bids at the balancing stage (cleared at minute-wise intervals). Besides, the model is enriched with a novel probabilistic constraint controlling the confidence level of the wind capacity offered to the reserve market.
2) To tackle the difficulty faced in representing the ultra-short-term wind uncertainty, the ACWGAN model is employed, for the first time, to generate effective scenarios for wind deviations conditioned on wind fluctuation levels. For this purpose, the definition of the new ACWGAN loss function and the connection of its three agents, i.e., critic, classifier, and generator, are used to construct its computational graph. Then, the architecture of each agent of ACWGAN is carefully designed to boost the performance of the proposed scenario generation while avoiding any pre-processing of the input data. The performance of the proposed scenario generation method is compared to other GAN-based alternatives in terms of statistical and similarity metrics.
3) The obtained wind speed trajectories with high temporal granularity, using ACWGAN, are then converted to power scenarios by an intermediate conversion layer comprising a penalized cubic B-spline method. Finally, the obtained ultra-short-term wind power scenarios are incorporated into the proposed data-driven probabilistic bidding framework. Accordingly, the proposed combinatorial contribution optimally leverages the benefits of both individual contributions by adopting the new ACWGAN scenario generation with the multi-resolution trading formulation. We show that the acquired optimal bids not only enhance the WPP profit in the market but also satisfy the required confidence level concerning reserve availability.

Comprehensive case studies and comparisons are conducted on real-world datasets. In particular, we quantify the loss of profit and deviation of the real-time reserve unavailability risk from the reserve market participation requirement when the model is fed by other GAN-based scenario generation techniques or scenarios from the direct random sampling method. In addition, the superiority of the proposed multi-resolution probabilistic bidding framework over the classic single-resolution and the ones without probabilistic constraint regarding reserve availability is highlighted.

The remainder of the paper is organized as follows. Section II describes the proposed multi-resolution two-stage stochastic WPP bidding framework with probabilistic constraint. Section III presents the details of the proposed ACWGAN model used to generate wind speed time trajectories with one-minute resolution. Section IV provides the numerical results. Finally, Section V concludes the paper.

II. Proposed Energy and Reserve Bidding Framework

This section first introduces the market mechanisms used in the DERM and then formulates the proposed WPP bidding strategy to obtain the optimal trade-off between reserve and energy shares based on the scenarios of wind power production.

A. Market Assumptions

Transmission System Operator (TSO) is responsible for maintaining the equilibrium between supply and demand to support grid stability. In the current market design, TSO transfers part of this responsibility to balance responsible parties (BRPs) in terms of financial liability. In this way, each BRP is subjected to imbalance tariffs for deviations of its actual energy delivery from balanced schedules (reported to TSO for every settlement period of the next day). In this study, in line with Finnish, Swedish, and

Danish market settings, the imbalance settlement and day-ahead market periods are considered to be one-hour [24]. The most commonly used imbalance settlement mechanisms in real-world electricity markets include single and dual pricing [2], [3]. Single pricing, e.g., used in Belgium and Germany, refers to the settlement procedure in which the BRPs with energy deficit have to pay the same imbalance price as the BRPs with generation surplus [3]. In contrast, dual pricing, e.g., used in Denmark, and Finland, which is applied in this study, penalizes net generation surpluses and deficits with different prices to create a better incentive for the BRPs to remain in balance [2].

However, in the case of real-time mismatch between supply and demand at the system level, the TSO relies on various capacity services that are purchased from balance service providers (BSPs) in the reserve market. In line with the real-world European electricity markets, in this study, the energy and reserve markets are cleared sequentially via independent day-ahead auctions [25], [26].

The BSPs should comply with balancing rules concerning the offered flexibility. This study focuses on frequency containment reserve (FCR), which has the fastest time response in the balancing market. The capacity test control requires the FCR providers to deploy the submitted capacity within one minute [27]. Therefore, as the obligation of means entails, the TSO should have access to the FCR provider's measurements and control system states to verify the availability of the offered capacity within the one-minute resolution [27]. Consequently, the BSP should satisfy the confidence level of the scheduled reserve bid. Deviations from the offered FCR are financially settled in the balancing stage. We consider a balancing market wherein one-directional upward FCR bids are also acknowledged as downward reserve provision for WPPs is not economically encouraged (since they do not leverage fuel-saving returns as conventional units do). Also, it is assumed that the WPPs' bids are accepted in the DERM due to their low marginal cost of power production [8].

B. Proposed WPP Bidding Framework

Although in this study the DERM is cleared sequentially, there still exists a strong relationship between the contribution of WPP in the energy-only and reserve markets [25]. This dependency is due to the capacity constraint, hourly and minute-wise wind uncertainty, coupling constraint of the uncertainty in different time scales, and risk of real-time reserve unavailability. Therefore, on account of this interdependency, and the short delay between the clearing of day-ahead energy and reserve markets [26], as a common approach in the dedicated literature [8]–[12], this section formulates a single decision-making problem for WPP bidding to achieve the optimal trade-off between the energy and reserve shares based on the scenarios of wind uncertainty.

The revenue of a WPP in the DERM, $\mathcal{R}$, consists of its contribution to the day-ahead market and real-time financial liability mechanisms. The day-ahead revenue is modeled at the first stage while real-time financial compensation is modeled at the second stage. The objective function of the proposed WPP bidding strategy is (1) shown at the bottom of this page.

The decision variables of the optimization problem include non-negative decision variables of the first stage $\mathrm{X} = \{P_t^{Eo}, P_t^{Ro}\}$, non-negative second-stage variables $\Psi = \{p_{\omega,t}^{E}, \Delta p_{\omega,t}^{E\downarrow}, \Delta p_{\omega,t}^{E\uparrow}, p_{\omega,(\nu,\delta),t}^{R}, \Delta p_{\omega,(\nu,\delta),t}^{R}, r_t\}$ and the auxiliary binary variables $\{z_{\omega,(\nu,\delta),t}\}$ regarding the second stage. The first term in (1), (i), presents the day-ahead profit of bidding in the DERM. The second term (ii) obtains the financial compensation in the energy imbalance settlement considering hourly wind power scenarios ω and corresponding energy deficits $\Delta p_{\omega,t}^{E\downarrow}$ and surpluses $\Delta p_{\omega,t}^{E\uparrow}$ for market periods. The last term (iii) reflects the balancing stage penalties considering wind mean deviation scenario (ν, δ) and scarcity of the allocated capacity $\Delta p_{\omega,(\nu,\delta),t}^{R}$ for market periods. $|\,.\,|$ indicates the cardinality of its set argument. All instances of time-series scenario ν, (ν, δ), have an identical probability for a given hourly wind scenario ω and market period *t*, i.e., $\mu_{\omega,\nu,t}$.

At this stage, it is important to note that a forecaster is firstly used to generate $|\Omega|$ hourly wind power scenarios to hedge against the uncertainty regarding real-time energy deviations. Then, an ACWGAN model is used to construct, around each mean hourly scenario $\omega \in \Omega$, $|V|$ scenarios of wind deviations, with length $|\Delta|$, regarding each one-minute interval $\delta \in \Delta$, inline with balancing stage periods.

The total submitted bids to the day-ahead market, should be within the upper $\bar{P}$ and lower $\underline{P}$ capacity limits of the WT.

$$\underline{P} \leq P_t^{Eo} + P_t^{Ro} \leq \bar{P} \;\; \forall\, t \in T \tag{2}$$

Then, (3) and (4) ensure that the allocated reserve in scenario ω and interval δ of mean deviation scenario ν for period *t*, $p_{\omega,(\nu,\delta),t}^{R}$, does not exceed $\tilde{P}_{\omega,(\nu,\delta),t}$ and P_t^{Ro}, respectively.

$$p_{\omega,(\nu,\delta),t}^{R} \leq \tilde{P}_{\omega,(\nu,\delta),t} \quad \begin{matrix} \forall\, t \in T; \forall\, \omega \in \Omega \\ \forall\; (\nu,\delta) \in V \times \Delta \end{matrix} \tag{3}$$

$$p_{\omega,(\nu,\delta),t}^{R} \leq P_t^{Ro} \quad \begin{matrix} \forall\, t \in T; \forall\, \omega \in \Omega \\ \forall\; (\nu,\delta) \in V \times \Delta \end{matrix} \tag{4}$$

Along with (3)-(4), (5)-(6) model the absolute reserve allocation control strategy of WPP, which enable it to act close to conventional units since it prioritizes power delivery to the

$$\max_{\mathrm{X},\Psi} \mathcal{R} = \sum_{t\in T} \Bigg[\underbrace{\lambda_t^{Eo} P_t^{Eo} + \lambda_t^{Ro} P_t^{Ro}}_{\text{(i)}} + \sum_{\omega\in\Omega} \pi_{\omega,t} \underbrace{\left(\lambda_t^{\uparrow} \Delta p_{\omega,t}^{E\uparrow} - \lambda_t^{\downarrow} \Delta p_{\omega,t}^{E\downarrow}\right)}_{\text{(ii)}} \underbrace{- \lambda_t^{R} |\Delta|^{-1} \sum_{\nu\in V} \mu_{\omega,\nu,t} \sum_{\delta\in\Delta} \Delta p_{\omega,(\nu,\delta),t}^{R}}_{\text{(iii)}} \Bigg] \tag{1}$$

reserve market [9], [11].

$$p^{R}_{\omega,(\nu,\delta),t} \geq P^{Ro}_{t} - \mathrm{M} z_{\omega,(\nu,\delta),t} \qquad \begin{matrix} \forall\, t \in T; \forall\, \omega \in \Omega; \\ \forall\ (\nu,\delta) \in V \times \Delta \end{matrix} \tag{5}$$

$$p^{R}_{\omega,(\nu,\delta),t} \geq \tilde{P}_{\omega,(\nu,\delta),t} - \mathrm{M}\left(1 - z_{\omega,(\nu,\delta),t}\right) \qquad \begin{matrix} \forall\, t \in T; \forall\, \omega \in \Omega; \\ \forall\ (\nu,\delta) \in V \times \Delta \end{matrix} \tag{6}$$

When available power is adequate, $\tilde{P}_{\omega,(\nu,\delta),t} \geq P^{Ro}_{t}$, $z_{\omega,(\nu,\delta),t}$ becomes zero to comply with (4) and avoid inconsistent constraints (4)-(6). In this regard, (4) imposes an upper limit, which is P^{Ro}_{t}, on $p^{R}_{\omega,(\nu,\delta),t}$ and thus the real-time allocated reserve power $p^{R}_{\omega,(\nu,\delta),t}$ matches the day-ahead reserve bid. However, when the available power is lower than the scheduled bid, $z_{\omega,(\nu,\delta),t}$ becomes equal to one, and (3) becomes an active constraint, thereby imposing an upper limit, i.e., $\tilde{P}_{\omega,(\nu,\delta),t}$, on $p^{R}_{\omega,(\nu,\delta),t}$. Thus, all available power is allocated to the reserve market, so as to reduce the reserve deviation penalty.

Then, the scarcity of the allocated reserve power $\Delta p^{R}_{\omega,(\nu,\delta),t}$ with respect to P^{Ro}_{t} is obtained by (7).

$$P^{Ro}_{t} - p^{R}_{\omega,(\nu,\delta),t} \leq \Delta p^{R}_{\omega,(\nu,\delta),t} \qquad \begin{matrix} \forall\, t \in T; \forall\, \omega \in \Omega; \\ \forall\ (\nu,\delta) \in V \times \Delta \end{matrix} \tag{7}$$

Importantly, since the proposed bidding framework considers wind uncertainty with two different time-scales, constraint (8) links the minute-wise and hourly scenarios, as follows:

$$p^{E}_{\omega,t} = \widetilde{\tilde{P}}_{\omega,t} \ - \ (|V|.|\Delta|)^{-1} \sum_{(\nu,\delta)\in V\times\Delta} p^{R}_{\omega,(\nu,\delta),t} \qquad \begin{matrix} \forall\, t \in T; \\ \forall\, \omega \in \Omega \end{matrix} \tag{8}$$

Note that the mean of ultra-short-term scenarios V regarding each hourly scenario ω at hourly time-period t ($(|V|.|\Delta|)^{-1}\sum_{(v,\delta)\in V\times\Delta}\tilde{P}_{\omega,(\nu,\delta),t}$) is equal to $\widetilde{\tilde{P}}_{\omega,t}$ as they also have a length of 1-hour and zero means. Accordingly, the decision variables can be separated into only two stages since scenarios of Ω can be alternatively obtained by V. However, employing hourly scenarios is still essential not only because of energy imbalance settlement, which occurs every hour, but also due to the fact that hourly scenarios can be obtained more accurately than wind scenarios with ultra-short-term variations (as will be further explained in section III). Notably, the first stage variables, which should be decided upon before the actual realization of the uncertainty in day-ahead, contribute to the strategic decision of the WPP regarding $P^{Eo}_{t}$and P^{Ro}_{t}. On the other hand, once the uncertainty is realized, operational decisions are taken at the second stage. Accordingly, since absolute reserve allocation strategy prioritizes power delivery to the reserve market, i.e., enforced by (3)-(6), the operational decision initially contains the allocation of reserve capacity regarding minute-wise wind scenarios for multiple time horizons, $|\Delta| = 60$. Concurrently, the remaining hourly mean power, which is obtained by (8), is then allocated to the real-time energy market. Consequently, operational decisions considering both hourly and minute-wise wind power uncertainties are made at the same stage (second stage).

The deficit and surplus of allocated powers to the energy market, used for energy imbalance settlement, are obtained by (9).

$$P^{Eo}_{t} - \ p^{E}_{\omega,t} = \Delta p^{E\downarrow}_{\omega,t} \ - \Delta p^{E\uparrow}_{\omega,t} \quad \forall\, t \in T; \forall\, \omega \in \Omega \tag{9}$$

Furthermore, as the proposed framework aims to satisfy the reliability of the offered reserve bids, the following constraint is given to approximate the risk of reserve unavailability:

$$r_t = \ |\Delta|^{-1} \sum_{\omega\in\Omega} \pi_{\omega,t} \sum_{(\nu,\delta)\in V\times\Delta} \mu_{\omega,\nu,t}\ z_{\omega,(\nu,\delta),t}\ \forall\, t \in T \tag{10}$$

As seen in (10), the probability-weighted average of the instances of power scarcity, $z_{\omega,(\nu,\delta),t} = 1$, with respect to the probability of hourly $\pi_{\omega,t}$ and minute-wise $\mu_{\omega,\nu,t}$ scenarios, estimates r_t.

Finally, the risk behavior of the WPP is controlled by defining an upper bound on the reserve market participation requirement, ρ^{o}_{t}, for each market time-unit, as follows:

$$r_t \leq \rho^{o}_{t} \quad \forall\, t \in T \tag{11}$$

It should be noted that although it is the TSO that defines ρ^{o}_{t} regarding the probability of reserve unavailability, WPP may take a lower risk depending on market incentives and wind power uncertainty to obtain the optimal allocation trade-off in each market floor.

It is worth noting that the single-resolution model, i.e., classic model, can be interpreted as a simplified version of the proposed framework wherein the ultra-short-term wind stochasticity is ignored. Particularly, the classic bidding model can be obtained by setting $\tilde{P}_{\omega,(\nu,\delta),t} = \widetilde{\tilde{P}}_{\omega,t}$ and $|V|, |\Delta|$, and $\mu_{\omega,\nu,t}$ to 1. Also, by removing (10)-(11) the bidding model neglects the confidence level of the offered reserve availability.

It should be emphasized that in this study, as in [4], [5] and [8]–[12], WPP is considered as a price-taker market participant, thereby market prices are not a function of its bids. Moreover, it can be seen that market rates enter linearly into the utility function (1). Consequently, provided that price forecast errors follow a normal distribution or numerous samples are available, to apply the central limit theorem, the stochasticity of market rates can be substituted with their expected values [5], [9], [11], [12]. It is worth noting that, as shown in [28], this simplification is still an acceptable approximation even if the forecast errors follow a gamma distribution and the utility function is to some extent nonlinear. In practice, since market rates are not known in advance, their corresponding values can be replaced by appropriate forecasts [5].

The wind power inter-temporal dependency between market periods *t* does not appear explicitly in the formulation, since they are already considered implicitly by the hourly scenarios fed to the framework. Thus, for the following reasons, the proposed framework can be decomposed into $|T|$ mixed-integer linear subproblems, for each *t*, to enhance the tractability of the proposed bidding framework. First, the paper focuses on the impact of wind uncertainty at the short-term, e.g., hourly, and ultra-short-term, e.g., minute-wise, resolutions on the bidding and reliability of the reserve power. Also, the chance constraints regarding reserve availability (10)-(11) are considered separately

for each individual market period *t*. The advantage of employing individual chance constraints over the joint chance constraints is that the reserve reliability in the former one is guaranteed over each market period, which is an important concern for TSO, rather than just for the whole day-ahead market.

III. Scenario Generation With ACWGAN

A wind speed time-trajectory $\tilde{w}_t$ with $|\Delta|$ samples per hour at a given hourly period t can be explicitly expressed via its hourly mean value $\bar{w}_t$ and ultra-short-term mean deviations ε_t by $\tilde{w}_t = 1\bar{w}_t + \varepsilon_t$; where $\mathbf{1}$ is a vector of all ones; $\mathbf{1}$ and ε_t are both $|\Delta| \times 1$ dimension.

A great effort is devoted to hourly wind forecast and scenario generation tools in the literature [29]–[33]. In general, since hourly wind variations and the required prediction horizon are both tractable, these methods yield acceptable performance [29], [30]. The required hourly wind scenarios Ω for the proposed bidding framework can be obtained by any of these effective methods, e.g., random sampling from the empirical hourly wind distribution [31] or probabilistic hourly wind speed forecast [32]. In this study, without loss of generality, the distribution of hourly wind forecast errors is used to represent the stochasticity of wind regarding $\bar{w}_t$. Remarkably, the distribution of wind frequency, especially in the medium- and long-term horizons, is conventionally fitted to the Weibull distribution [33]. Also, it can be better modeled with the non-parametric approaches [34]. In this study, the hourly wind uncertainty is represented by a normal distribution as in the wind-related literature on stochastic programming [31].

Nevertheless, generating efficient zero mean wind deviation scenarios with a high temporal resolution, concerning ε_t, is challenging [11], [12]. This increased difficulty is primarily due to the higher randomness and volatility of wind over ultra-short time periods (e.g., minute-wise) compared to short-term periods (e.g., hourly) [29], [30]. Moreover, in this study, the required prediction horizon for the wind deviation scenarios with high temporal granularity is $|\Delta|$ (i.e., $= 60$) times more than the short-term scenarios.

Therefore, this section proposes a new model to capture the time-varying and nonlinear dynamics of high-dimensional weather data regarding ultra-short-term wind variations by learning their distribution directly without making any modeling assumptions. The proposed model for generating wind scenarios with high temporal granularity consists of three agents, i.e., critic, generator, and classifier. Unlike previous ACWGAN models [19], [20], which use the trained critic for a classification problem, we use the generator to create effective wind scenarios. Therefore, with respect to our particular application, we explain the relevance of the ACWGAN agents and their connections in the computational graph so as to train the entire model with the new learning loss feedback developed for each agent. To provide a better perspective, in this section, we detail step by step the advantages of the proposed scenario generation tool beyond the state of the art by highlighting the limitations of other similar GAN-based models used for this purpose.

A. Wasserstein GAN With Gradient Penalty

A GAN consists of an interconnected network comprising a generator $G_\alpha(.)$ and discriminator $D_\beta(.)$ which simultaneously compete in a zero-sum game. $G_\alpha(.)$ samples a latent noise vector $\mathcal{Z}$ from the latent space with the probability distribution $\mathcal{P}_\mathcal{Z}$, i.e., $\mathcal{Z} \sim \mathcal{P}_\mathcal{Z}$, as input and attempts to map it to realistic-looking data s_g, e.g., scenario of wind time-series, in the output $G_\alpha(\mathcal{Z})$. Notably, $\mathcal{Z}$ should have a relatively low dimension to facilitate the generator's task in mapping the latent space to $\mathcal{P}_r$ [35]. $D_\beta(.)$ receives either a real sample $s_r \sim \mathcal{P}_r$ drawn from the original dataset, e.g., actual wind dataset, or synthesized sample $s_g \sim \mathcal{P}_g$, as input and identifies its realness or fakeness. On the other hand, $G_\alpha(.)$ aims to generate realistic-looking samples, e.g., wind time-series scenarios, to deceive $D_\beta(.)$. GAN is trained by using binary cross-entropy loss function in a zero-sum game [18].

Remarkably, GAN's loss function can be interpreted as minimizing Jensen-Shannon Divergence (JSD) between $\mathcal{P}_r$ and $\mathcal{P}_g$ [36]. However, JSD fails to provide a sensible gradient in GAN training when distributions have non-overlapping support [17]. This undesirable characteristic of JSD leads to several issues, such as training instability and mode collapse in GAN's training process [36]. To circumvent these drawbacks, a Wasserstein distance-based loss function is proposed in [37]. Also, adopting such a loss function prevents the potential overfitting problem of the model [37]. The improved loss function in WGAN, by converting WD problem to its dual form, for better computational tractability, is as follows [38]:

$$\begin{aligned}\mathcal{L}_W\left(D_\beta, G_\alpha\right) &= \min_{\alpha} \max_{\beta} \mathbb{E}_{s_r \sim \mathcal{P}_r}\left[D_\beta\left(s_r\right)\right] \\ &\quad - \mathbb{E}_{s_g \sim \mathcal{P}_g}\left[D_\beta\left(s_g\right)\right] \\ &\quad - \eta_{GP} \mathbb{E}_{\hat{s} \sim \hat{\mathcal{P}}}\left[\left(\nabla_{\hat{s}} \| D_\beta\left(\hat{s}\right)\|_2 - 1\right)^2\right] \quad (12)\end{aligned}$$

where $\hat{s}$ symbolizes the linearly interpolated data points belonging to $\mathcal{P}_r$ and $\mathcal{P}_g$, which is defined as follows:

$$\hat{s} = \theta s_r + (1-\theta)\, s_g \; s_r \sim \mathcal{P}_r \; ; \; s_g \sim \mathcal{P}_g ; \; \theta \sim U\left[0,1\right] \quad (13)$$

In WGAN, the so-called critic $D_\beta(.)$ measures the discrepancy between $\mathcal{P}_r$ and $\mathcal{P}_g$, e.g., the discrepancy between actual and generated wind time-series, through Wasserstein metric $WD(\mathcal{P}_r, \mathcal{P}_g)$ by inner maximization in (12). On the other hand, $G_\alpha(.)$ tries to produce realistic-looking data by minimizing $WD(\mathcal{P}_r, \mathcal{P}_g)$ through the outer minimization in (12).

B. Conditional Wasserstein GAN

Despite the satisfactory performance of the discussed generative models in providing realistic-looking scenarios, they still fail to control the features or modes, e.g., wind deviation levels, of the generated data. Nevertheless, this limitation can be tackled by integrating supplementary information, e.g., class labels, into the adversarial training process of GAN variants.

Particularly, in the critic's network $D_\beta(.|c)$ of CWGAN, the class labels $c \sim \mathcal{P}_c$ are merged with the actual $s_r \sim \mathcal{P}_r$ and generated $s_g \sim \mathcal{P}_g$ samples to obtain a joint hidden representation

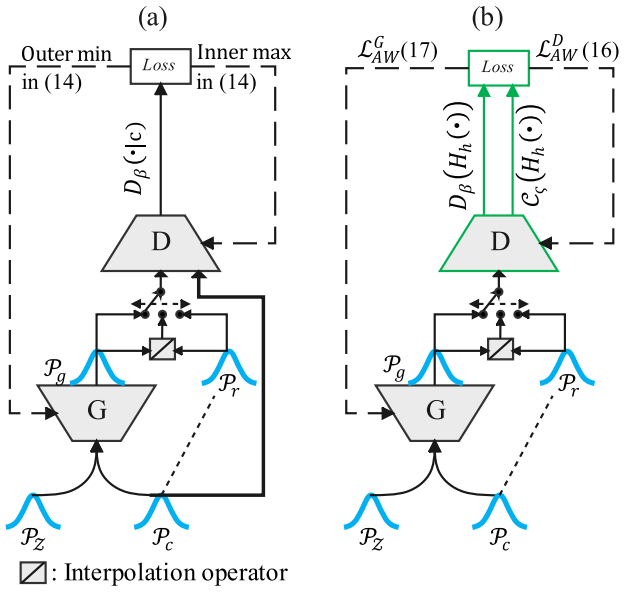

Fig. 1. Input-output diagram of (a): CWGAN, (b): ACWGAN.

of samples and class labels. Furthermore, in the generator's network, these class labels are merged with the latent noise vectors $\mathcal{Z} \sim \mathcal{P}_\mathcal{Z}$. The loss function of CWGAN, $\mathcal{L}_{CW}(D_\beta, G_\alpha)$, is then expressed as follows:

$$\begin{aligned}\mathcal{L}_{CW}\ (D_\beta, G_\alpha) \ = \ & \min_{\alpha} \max_{\beta} \ \mathbb{E}_{s_r \sim \mathcal{P}_r} \left[D_\beta \left(s_r|c\right)\right] \\ & - \mathbb{E}_{s_g \sim \mathcal{P}_g} \left[D_\beta \left(s_g|c\right)\right] \\ & - \eta_{GP} \mathbb{E}_{\hat{s} \sim \hat{\mathcal{P}}} \left[\left(\nabla_{\hat{s}} \| D_\beta \left(\hat{s}|c\right)\|_2 - 1\right)^2\right]\end{aligned} \tag{14}$$

The input-output diagram of CWGAN is shown in Fig. 1(a). It can be seen that the input of the critic in CWGAN encompasses class labels, highlighted by a bold black arrow, along with the joint hidden representation of class labels and input samples. CWGAN is practically trained by sequentially updating the critic and generator parameters, using the loss feedbacks, shown by dashed lines, through the inner maximization and outer minimization problems of (14), respectively.

C. Proposed Wasserstein GAN With Auxiliary Classifier

CWGAN learns a representation of $\mathcal{Z}$ that depends on class labels as it receives them as input to the network. In other words, CWGAN requires $D_\beta(.|c)$ to return an estimate of the distance between generated and real joint distributions of class labels and samples, by merging c to either $\mathcal{Z}$ or s_r, since it receives them as input. The complicated task of $D_\beta(.|c)$, measuring the discrepancy between the real and generated joint distributions, and $G_\alpha(.|c)$, mapping the latent space (which is further entangled by merging the class labels into $\mathcal{Z} \sim \mathcal{P}_\mathcal{Z}$) to real data distribution, can be alleviated by incorporating a new agent into the adversarial training process. This leads to an increase in the learning capacity of the model and thus to more effective scenarios, as the new agent provides for better classification accuracy. The additional agent, which is a classifier $\mathcal{C}_\varsigma(.)$ and cooperates with $D_\beta(.)$ and $G_\alpha(.)$, estimates the conditional probability of the class labels given the received samples. Thus, the critic now merely estimates the distance between real and generated data distributions, through $WD(\mathcal{P}_r, \mathcal{P}_g)$, which is independent of the class labels, e.g., wind deviation levels.

Moreover, the generator can better map $\mathcal{P}_\mathcal{Z}$ to $\mathcal{P}_r$ through $G_\alpha(.)$ as its loss function, $\min_\alpha -\mathbb{E}_{s_g \sim \mathcal{P}_g}[D_\beta(s_g|c)]$, depends on the critic's performance as well. Nevertheless, both the generator and critic should still contribute to enhancing the ability of $\mathcal{C}_\varsigma(.)$ to predict the class labels of the samples correctly. The proposed three-player adversarial loss function of ACWGAN, $\mathcal{L}_{AW}(G_\alpha, \mathcal{C}_\varsigma, D_\beta)$, can be formulated as:

$$\begin{aligned}\mathcal{L}_{AW}\ (G_\alpha, \mathcal{C}_\varsigma, D_\beta) \ = \ & \min_{\alpha} \min_{\varsigma} \max_{\beta} \ \mathbb{E}_{s_r \sim \mathcal{P}_r} \left[D_\beta \left(s_r\right)\right] \\ & - \mathbb{E}_{s_g \sim \mathcal{P}_g} \left[D_\beta \left(s_g|c\right)\right] \\ & - \eta_{GP} \mathbb{E}_{\hat{s} \sim \hat{\mathcal{P}}} \left[\left(\nabla_{\hat{s}} \| D_\beta \left(\hat{s}|c\right)\|_2 - 1\right)^2\right] \\ & - \ \eta_c \mathbb{E}_{s_r \sim \mathcal{P}_r} \left[\log \mathbb{P}\left(\mathcal{C}_\varsigma \ \left(s_r\right) = \ c\right)\right] \\ & - \ \eta_c \mathbb{E}_{s_g \sim \mathcal{P}_g} \left[\log \mathbb{P}\left(\mathcal{C}_\varsigma \ \left(s_g\right) = \ c\right)\right]\end{aligned} \tag{15}$$

where ς indicates the classifier's trainable parameters, c is the true class label of the received sample, and η_c is a hyperparameter regarding the weight of the log-likelihood loss, $\log \mathbb{P}(.)$, of the correct class prediction. The first three terms in (15) correspond to the WD of the generated and real data distributions which should be estimated by $D_\beta(.)$ through the inner maximization and minimized by $G_\alpha(.)$ via the outer minimization problem. The last two terms in (15) minimize the negative log-likelihood loss of the correct class prediction through the middle minimization problem.

In practice, the ACWGAN three-player game can be implemented by two neural networks comprising a new critic, which also embeds an auxiliary classifier layer as its secondary output, and a generator. In this way, the auxiliary classifier $\mathcal{C}_\varsigma(.)$ and critic $D_\beta(.)$ in (15) share the same hidden layers H_h, parameterized by h, in the new critic. Importantly, by leveraging the benefits of multi-task learning [39], such a structure improves the three-player ACWGAN learning performance and reduces its complexity. Particularly, the new critic receives an input sample, either from $\mathcal{P}_r$ or $\mathcal{P}_g$, and, in contrast to CWGAN, returns two outputs $[D_\beta(H_h(.)), \mathcal{C}_\varsigma(H_h(.))]$. The first output, $D_\beta(H_h(.))$, obtains the WD between real and generated distributions through the inner maximization in (15). However, the second output of the new critic in ACWGAN, $\mathcal{C}_\varsigma(H_h(.))$, predicts the class label of each provided sample rather than merely receiving it as an input (as in the case of CWGAN). The new critic's loss function is as follows:

$$\begin{aligned}\mathcal{L}_{AW}^D = \ & \max_{\{h,\beta,\varsigma\}} \ \mathbb{E}_{s_r \sim \mathcal{P}_r} \left[D_\beta \left(H_h \left(s_r\right)\right)\right] \\ & - \mathbb{E}_{s_g \sim \mathcal{P}_g} \left[D_\beta \left(H_h \left(s_g|c\right)\right)\right] \\ & - \eta_{GP} \mathbb{E}_{\hat{s} \sim \hat{\mathcal{P}}} \left[\left(\nabla_{\hat{s}} \| D_\beta \left(H_h \left(\hat{s}|c\right)\right)\|_2 - 1\right)^2\right] + \eta_c \mathbb{E}_{s_r \sim \mathcal{P}_r} \\ & \left[\log \mathbb{P}\left(\mathcal{C}_\varsigma \ \left(H_h \left(s_r\right)\right) = \ c\right)\right] \\ & + \ \eta_c \mathbb{E}_{s_g \sim \mathcal{P}_g} \left[\log \mathbb{P}\left(\mathcal{C}_\varsigma \ \left(H_h \left(s_g\right)\right) = \ c\right)\right]\end{aligned} \tag{16}$$

In (16), $WD(\mathcal{P}_r, \mathcal{P}_g)$ is estimated by the first three terms. The last two terms in (16) optimize the auxiliary classifier layer by inverting the sign of negative log-likelihood loss, regarding the middle minimization problem in (15), and expressing it as a maximization problem.

Nevertheless, in the same fashion as in CWGAN, the generator receives latent noise vectors along with class labels, e.g., wind deviation levels, and returns synthesized samples, e.g., scenario of wind time-series, holding desired class attributes. Accordingly, the generator aims to produce quality samples to reduce the discrepancy between the generated and real data distributions, i.e., by solving the outer minimization problem in (15). It is seen that only the second term in (15), $-\mathbb{E}_{s_g\sim\mathcal{P}_g}[D_\beta(s_g|c)]$, involves the generator's parameters regarding the minimization of $WD(\mathcal{P}_r, \mathcal{P}_g)$. By inverting its sign, the minimization problem can be converted to a maximization one. Notwithstanding, the synthesized samples by the generator should also have the correct class attributes. It is seen that only the last term in (15), $-\eta_c\mathbb{E}_{s_g\sim\mathcal{P}_g}[\log\mathbb{P}(\mathcal{C}_\varsigma(s_g) = c)]$, contains the generator's parameters regarding the correct class prediction error. Thus, by inverting its sign, the two mentioned contributing elements can be combined as follows to construct a single loss function $\mathcal{L}_{AW}^G$ for training the generator:

$$\mathcal{L}_{AW}^G = \max_{\alpha}\ \mathbb{E}_{s_g\sim\mathcal{P}_g}[D_\beta(H_h(s_g|c))] + \eta_c\mathbb{E}_{s_g\sim\mathcal{P}_g}[\log\mathbb{P}(\mathcal{C}_\varsigma(H_h(s_g)) = c)] \quad (17)$$

The input-output diagram of ACWGAN is shown in Fig. 1(b). It is seen that the new critic of ACWGAN, shown by a green block, does not receive class labels as input. Nevertheless, in contrast with the critic of CWGAN, the new critic of ACWGAN has two outputs, shown by green arrows. The first output, $D_\beta(H_h(\cdot))$, obtains the WD between real and generated distributions while the second output, $\mathcal{C}_\varsigma(H_h(\cdot))$, predicts the class label of the provided sample. Finally, ACWGAN is trained by sequentially updating the parameters of the new critic and generator through loss feedbacks $\mathcal{L}_{AW}^D$ and $\mathcal{L}_{AW}^G$, (shown by dashed lines), respectively.

The training process of ACWGAN is elaborated in detail in Algorithm I. Importantly, as seen in Algorithm I, at each training step, the new critic is first trained by few iterations, typically $n_d = 5$ [38], to estimate $WD(\mathcal{P}_r, \mathcal{P}_g)$ and improve the classifier's ability to correctly predict class labels of $s_r \sim \mathcal{P}_r$ and $s_g \sim \mathcal{P}_g$. During this step, the generator's parameters are not updated, since $\mathbb{E}_{s_g\sim\mathcal{P}_g}[D_\beta(H_h(s_g|c))]$ has different signs in the loss functions (16) and (17). Thus, after the new critic training, the generator is trained for one iteration to minimize the obtained WD through the first term in (17), i.e., maximizing $-WD(\mathcal{P}_r, \mathcal{P}_g)$, while satisfying the correct class property of generated samples as it is also considered in $\mathcal{L}_{AW}^G$. Notably, the new critic's parameters are not updated at this step, since training the critic with $\mathcal{L}_{AW}^G$ results in an inaccurate estimate of $WD(\mathcal{P}_r, \mathcal{P}_g)$ due to their conflicting objectives. This procedure is continued until the model is converged and desired outputs are achieved.

Once ACWGAN is trained by labeled samples, the generator is capable of producing plausible wind speed mean deviation scenarios with a high temporal resolution, e.g., minute-wise time granularity, and desired class labels, e.g., deviation levels. In this regard, the generator is fed by K noise vectors $\mathcal{Z}$ and desired class label c to obtain K scenarios of wind speed mean deviation with $|\Delta|$, e.g., $= 60$, samples per hour.

These effectively-controlled wind speed scenarios are then converted to wind power scenarios through an intermediate conversion layer. In this paper, a penalized cubic B-spline method which better controls the curvature of the fitted power curve is employed. In this method, a penalty term is added to the least square fitting objective in order to control the smoothness of the power curve. The details of this method are given in [23]. Nevertheless, more advanced techniques, e.g., neural networks, can be incorporated into the proposed speed to power conversion layer, to deal with a wind farm where its total production is significantly affected by other factors such as wake effects.

Finally, the WPP receives K effective realistic-looking wind power scenarios with a high temporal resolution as input to

Training Algorithm I: Proposed ACWGAN Model.

Default values: $n_b = 64$, $n_d = 5$, $\eta_{GP} = 10$, $\eta_c = 1$, Gradient descent optimizer = Adam , l_r =0.00006.

Require: n_b, Batch size. n_d, Number of critic's updates in ACWGAN. η_{GP}, Gradient penalty. η_c, Log-likelihood weight loss. Gradient descent optimizer. l_r, Learning rate.

Require: Initialize model's weights $\{\alpha, h, \beta, \varsigma\}$.

while weights have not converged **do:**

  ▸**Execute n_d training steps for the combined discriminator and classifier network.**

  for $n = 1, \ldots, n_d$ **do:**

    for $i = 1, \ldots, n_b$ **do:**

      Take a real sample along with its class label from $\mathcal{P}_r$.
      s_r and $c \sim \mathcal{P}_r$

      sample a noise vector from latent space $\mathcal{P}_z$.
      $z \sim \mathcal{P}_z$

      Generate fake sample using G_α.
      $s_g \leftarrow G_\alpha(z|c)$

      Obtain the interpolated sample $\hat{s}$.
      $\hat{s} \leftarrow \theta s_r + (1-\theta)s_g$, where $\theta \sim U[0,1]$

      Compute the combined discriminator and classifier loss regarding s_r, s_g and $\hat{s}$.

$$L_D(i) \leftarrow D_\beta(H_h(s_r)) - D_\beta\left(H_h(s_g|c)\right) - \eta_{GP}\left(\nabla_{\hat{s}}\left\|D_\beta(H_h(\hat{s}|c))\right\|_2 - 1\right)^2 + \eta_c\log\mathbb{P}\left(\mathcal{C}_\varsigma(H_h(s_r)) = c\right) + \eta_c\log\mathbb{P}\left(\mathcal{C}_\varsigma\left(H_h(s_g)\right) = c\right)$$

    end for

    Update discriminator and classifier layer parameters $\{h, \beta, \varsigma\}$ using gradient descend algorithm.

$$\{h, \beta, \varsigma\} \leftarrow \text{Adam}\left(-\nabla_{\{h,\beta,\varsigma\}}\, n_b^{-1}\sum_{i=1}^{n_b} L_D(i)\right)$$

  end for

  ▸**Execute a single generator training step.**

  Sample a batch of noise vectors and class labels.
  $\{z(i)\}_{i=1}^{n_b} \sim \mathcal{P}_z$; $\{c(i)\}_{i=1}^{n_b} \sim \mathcal{P}_c$

  Generate a batch of fake samples using the generator network.
  $\{s_g(i)\}_{i=1}^{n_b} \leftarrow G_\alpha(\{z(i)\}_{i=1}^{n_b}|\{c(i)\}_{i=1}^{n_b})$

  Update generator parameters α using gradient descend algorithm.

$$\alpha \leftarrow \text{Adam}\left(-\nabla_\alpha\, n_b^{-1}\sum_{i=1}^{n_b} D_\beta\left(H_h(s_g(i)|c(i))\right) + \eta_c\log\mathbb{P}\left(\mathcal{C}_\varsigma\left(H_h(s_g(i))\right) = c(i)\right)\right)$$

end while

TABLE I
PRICES AND PENALTY RATES OF THE STUDIED DERM PERIOD

λ^{Eo} [€/MWh]	λ^{Ro} [€/MW]	$\lambda^{\uparrow}$ [€/MWh]	$\lambda^{\downarrow}$ [€/MWh]	λ^{R} [€/MW]
33	35	31	36	40

the stochastic bidding model. These scenarios follow the actual wind dynamics due to the employed loss based on *WD*. More importantly, thanks to the embedded classifier in the ACWGAN training, the WPP also has control over the desired properties, e.g., deviation levels, of the generated scenarios.

IV. NUMERICAL RESULTS

This section conducts comprehensive case studies on real-world datasets, based on the experimental setups described in subsection IV.A. Since wind power variation scenarios are the inputs of the proposed multi-resolution probabilistic bidding framework, the performance of the proposed ACWGAN model is firstly compared to the other alternatives based on statistical and similarity metrics in subsection IV.B. Afterward, the advantages of the proposed data-driven probabilistic WPP energy and reserve scheduling framework, which models wind uncertainty with both hourly and one-minute resolutions, via ACWGAN, over the classic single-resolution model are investigated in subsection IV.C. Finally, the benefits of using ACWGAN in the presented decision tool, in contrast to the other alternative scenario representation methods, are further investigated in subsection IV.D.

A. Experimental Setups

A WPP owning a 5.3 MW wind turbine with cut-in, rated and cut-out speed of, respectively, 3, 12, and 25 m.s^{-1} is studied here. It should be noted that even with this limited wind power capacity, portfolios are still able to participate at both day-ahead energy and reserve market floors. For example, in the electricity markets operated by EPEX-Spot and Nord Pool (which include several countries, such as Belgium), the minimum bid size in the day-ahead energy market is 0.1 MW [40]. Also, in many countries, such as Belgium, Denmark, and France, the portfolios with at least 1 MW of flexible power are allowed to participate in the balancing market as BSP [41]. The hourly wind scenarios are obtained by sampling from a normal distribution with the mean wind speed of 9 m.s^{-1} and standard deviation of 1.5 m.s^{-1}. Notably, this assumption does not affect our comparisons since all benchmarks and the proposed method are fed by the same hourly wind scenarios. Furthermore, the ultra-short-term wind scenarios are obtained by ACWGAN and evaluated by other benchmark algorithms including direct random sampling from the training set, CGAN, and CWGAN. Both hourly and ultra-short-term scenarios, employed in the proposed bidding framework, are considered equiprobable. Market prices and penalties for one market period are reported in Table I. These market rates are in a similar and comparable range as in the related literature [11], [12] and in several European electricity markets, such as in Denmark, Norway, and Belgium [42], [43].

The reserve unavailability penalty rate during each imbalance settlement period is constant. The proposed scheduling problem is solved for one market period. This reduction is not limiting as one can solve the problem for $|T|$ market periods by decomposition of (1)-(11) as detailed in Section II.B. Moreover, this setting allows us to better demonstrate the effectiveness of the proposed approach by detailing various aspects of in- and out-of-sample results.

In this study, a sufficiently large dataset regarding minute-wise and hourly wind variations from 2014 to 2016 is collected from a wind site located in Frøya island [44]. Specifically, the wind dataset contains 453600 instances regarding 7560 hours of minute-wise wind data. The processed dataset is then divided into training and test sets with a 4:1 ratio.

For the sake of a fair comparison, the same type of neural network is used for the critic (discriminator) and generator of all GAN-based methods. Specifically, the architecture of the generator neural network involves three fully connected layers, whereas the critic (discriminator) uses three one-dimensional convolution layers. Moreover, the number of neurons in the hidden layer of each network for each model is fine-tuned based on 50 trial runs. The neural networks are trained with 362880 data instances corresponding to 6048 hours of wind data, i.e., each sample has $(|\Delta| = 60)\times 1$ dimension (one dimension per minute), along with their associated labels. Notably, the model can be trained by any auxiliary information such as seasons, ramping rate, or deviation level. In this study, wind fluctuation level is adopted as our supplementary information, which can be provided by a forecaster, as it has a significant impact on optimal decisions of the bidding model. In this study, the fluctuation levels are divided into 5 categories with respect to the distribution of wind variability in the training set.

In particular, the fluctuation levels belonging to intervals [0, 0.5), [0.5, 1), [1, 1.5), [1.5, 2) and [2, S_{max}] m.s^{-1} corresponds to the class labels C_o, C_1, C_2, C_3, and C_4, respectively. S_{max} denotes the maximum wind deviation value and is 5 m.s^{-1} in our dataset. Notably, C_o, C_1, and C_2, with the probability of, respectively, 0.37, 0.40, and 0.15, are the dominant events in the dataset. On the other hand, C_3 and C_4, with the probability of, respectively, 0.03, and 0.05 are less probable events. After training the models, the standalone generator is fed by $K = 1000$ noise vectors along with desired class labels to produce appropriate wind mean deviation scenarios in the form of time trajectory. For the sake of method evaluation, a sufficiently large number of samples, i.e., 5000, with $K = 1000$ samples for each class, are generated. Then, the out-of-sample analysis is performed over the expectation of 75650 instances regarding 1513 hours of wind data in the test set.

B. Evaluation of the Proposed Scenario Generation Model

Although the evaluation of GAN-based models with image output is rather straightforward, their evaluation for non-image data is still an open topic [45]. Therefore, various similarity and statistical metrics, based on specific applications, are employed in the literature to assess the performance of time-series generative models. First, Wasserstein distance, *WD*, between

the probability distributions of the generated $\mathcal{P}_g$ and test sets $\mathcal{P}_r$ instances of wind trajectories, for each label, is calculated as follows (to compare the overall variability of two sets):

$$WD\ (\mathcal{P}_r, \mathcal{P}_g\ ) = \inf_{\gamma \in \Gamma(\mathcal{P}_r, \mathcal{P}_g)} \mathbb{E}_{(s_r, s_g)\sim\gamma} \|s_r - s_g\| \quad (18)$$

Then, the root-mean-square error (RMSE) of the generated and test sets are computed. The RMSE between two temporal sequences, f and $\hat{f}$, is defined as follows:

$$\text{RMSE}\ \left[f, \hat{f}\right] = \sqrt{|\Delta|^{-1} \sum\nolimits_{\delta\in\Delta} \left(f\left[\delta\right] - \hat{f}\left[\delta\right]\right)^2} \quad (19)$$

Finally, dynamic time-warping (DTW), a well-known time-series similarity metric, is also used to analyze the similarity of time-series in the generated and test sets with respect to the optimal alignment of time warps [46]. Let's $d_{i,j} = \|f[i] - \hat{f}[j]\|\ ,\ i, j \in \Delta$ be the local cost of alignment between the i^{th} element of f and the j^{th} element of $\hat{f}$. A warping path $\langle W\ = \langle w_1, \ldots, w_L\rangle\ \mid L \in [|\Delta|, 2|\Delta| + 1]\rangle$, encodes a global alignment between the two time-series, f and $\hat{f}$, by defining a sequence of L pairs $w_l = (i, j)$, which assign element i of f to element j of $\hat{f}$. The DTW distance between two time-series is the total cost of alignment for the optimal (i.e., minimum cost) warping path:

$$\text{DTW}\ \left[f, \hat{f}\right] = \min_{W} \sum_{l=1}^{L} \tilde{d}_l\ W = \langle w_1, \ldots, w_L\rangle \quad (20)$$

where $\tilde{d}_l = d_{i,j}$ is the local alignment cost encoded by the l^{th} pair $w_l = (i, j)$ of the warping path W.

DTW and RMSE are conventionally used to evaluate the quality of the generated signals in GAN models [46]. Two real wind trajectories are randomly chosen from the test dataset as shown by black lines in the first and second columns of Fig. 2. Then, after generating a set of wind trajectories by using ACWGAN, CWGAN, and CGAN, the most similar synthesized wind time-series based on RMSE and DTW metrics are found. The actual wind time-series in the first and the second columns are used to obtain the most similar synthesized sample with respect to RMSE and DTW metrics, respectively. The obtained synthesized trajectories using ACWGAN, CWGAN, and CGAN regarding RMSE metric are, respectively, shown in Fig. 2(a), (c), and (e) by dashed blue lines. Also, the dashed blue lines in Fig. 2(b), (d), and (f) correspond to the obtained trajectories using ACWGAN, CWGAN, and CGAN regarding DTW, respectively. It is seen that while the synthesized samples in the left column emphasize the static time alignment, the ones in the right column relax this assumption by using dynamic time alignment. Additionally, the corresponding generated trajectories using ACWGAN, as shown in Fig. 2(a) and (b), are visually similar to the ones belonging to the real dataset for both RMSE and DTW metrics. On the other hand, the generated samples using CWGAN are visually less similar to the ones belonging to the real dataset, compared with the generated samples by ACWGAN, regarding both similarity metrics. Also, the obtained samples by CGAN even look farther than their corresponding real samples compared with the ones obtained by ACWGAN and

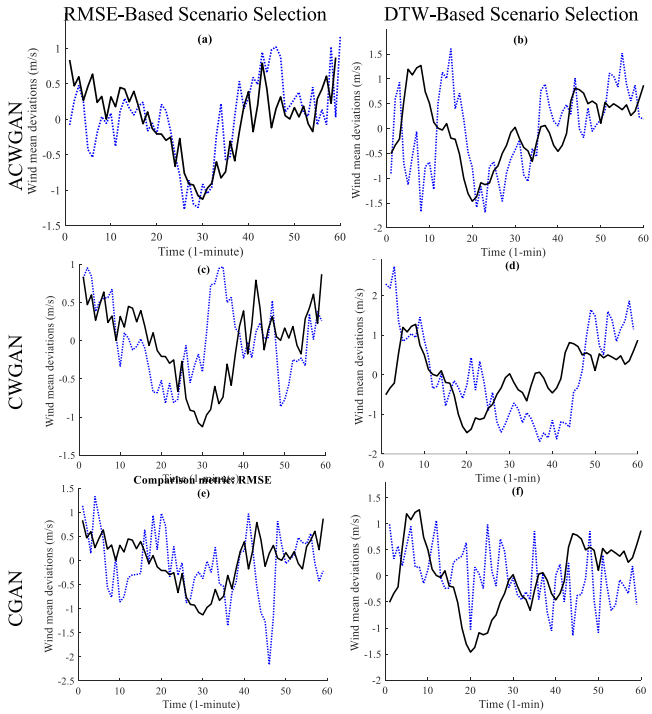

Fig. 2. Generated wind mean deviation time-series versus the actual time-series. The first and second columns correspond to the scenarios selected based on RMSE and DTW metrics, respectively. The generated signals using ACWGAN, CWGAN, and CGAN are, respectively, shown in rows 1, 2, and 3.

CWGAN. In particular, the RMSE between the real signals (first column) and the generated signals by ACWGAN, CWGAN, and CGAN are 0.47, 0.63, 0.75, respectively. Also, the DTW between the real signals (second column) and the generated signals by ACWGAN, CWGAN, and CGAN are 21.70, 28.62, 30.17, respectively.

Nevertheless, DTW and RMSE merely find the distance of two temporal sequences, which are used for qualitative visual assessment in Fig. 2. Thus, it is required to obtain representative scores based on these metrics for the whole generated scenarios on the test dataset. For this purpose, a brute-force search on the synthesized and test sets is performed to find the most similar time-series based on the desired metric. Then, the average of the obtained cost values, i.e., RMSE and DTW, of the corresponding similar signals in real and generated datasets are considered to obtain the representative RMSE and DTW distance of two sets. The acquired results for the mentioned evaluation metrics on the whole datasets are recorded in tuples (WD, RMSE, DTW) in Table II. The performance of each presented method should be compared with other methods for each class label individually.

It can be seen that CGAN performs poorly with respect to all measures compared to CWGAN and ACWGAN. Moreover, the performance of the proposed ACWGAN is considerably better compared to CWGAN.

For example, as seen in the 4$^{\text{th}}$ row of Table II, i.e., C_3, WD, RMSE and DTW of ACWGAN are 1.89, 1.55 and 1.30 times lower than those of CWGAN method, indicating higher quality of scenarios generated by the proposed method.

TABLE II
COMPARISON OF THE PROPOSED SCENARIO GENERATION APPROACH WITH THE OTHER GAN-BASED TECHNIQUES

Class \ Method	CGAN	CWGAN	ACWGAN
Co	(0.14, 0.24, 18.20)	(0.04, 0.11, 9.33)	(0.04, 0.10, 8.95)
C_1	(0.07, 0.43, 23.97)	(0.05, 0.37, 17.19)	(0.05, 0.31, 16.84)
C_2	(0.15, 1.44, 42.94)	(0.07, 0.95, 30.22)	(0.06, 0.89, 28.75)
C_3	(0.17, 3.64, 67.17)	(0.17, 2.73, 49.52)	(0.09, 1.76, 38.22)
C_4	(0.96, 12.61,138.50)	(0.20, 3.87, 57.64)	(0.13, 3.31, 55.22)

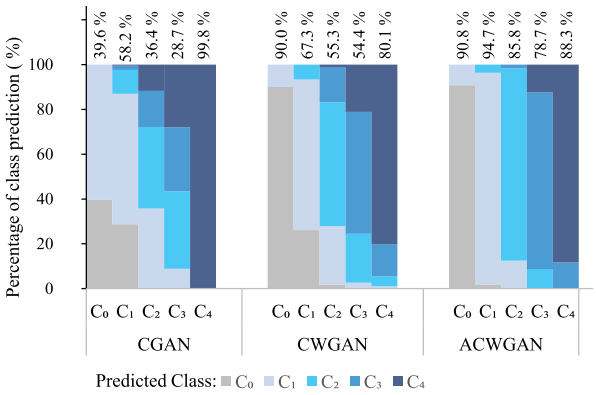

Fig. 3. Confusion matrix of CGAN, CWGAN, and ACWGAN regarding class labels C_o, C_1, C_2, C_3, and C_4.

The ACWGAN model is further compared with the benchmark models in terms of classification performance. For this purpose, the 5000 generated samples, i.e., 1000 samples for each class, are analyzed ex-post in order to obtain their confusion matrix, as shown in Fig. 3. The predicted classes are color-coded in this figure. The horizontal axis shows the true class labels. Hence, each bar segment in a given stacked bar indicates the percentage of predicted classes for each true class label. It is graphically seen that CGAN has poor performance compared to the Wasserstein-based models for C_o, C_1, C_2, and C_3. However, its performance regarding generating wind time-series with class label C_4 is better than the Wasserstein-based models. Its reason can be described as below.

Notably, C_4 has a much wider interval [2, S_{max}] compared to other classes (3 m.s^{-1} vs. 0.5 m.s^{-1}). Meanwhile, the deviation levels of wind time-series belonging to C_4 in the real dataset are mostly concentrated toward the beginning, and middle of this interval. On the other hand, the deviation levels of the generated time-series by CGAN are mostly concentrated on the right tail of C_4 interval (higher deviation level). Thus, although the classification accuracy of CGAN regarding C_4 seems to be improved, as the deviation levels still fall in this wide interval, they do not maintain the quality of the real wind signals of this class. This can be further confirmed by the poor results of CGAN regarding C_4, with respect to the similarity metrics, as reported in Table II.

TABLE III
THE IN- AND OUT-OF-SAMPLE RESULTS OF THE PROPOSED AND CLASSIC BIDDING APPROACHES FOR DIFFERENT ρ^o AND WIND DEVIATION CLASSES

			In-sample				Out-of-sample			Evaluation	
	ρ^o [%]	Method	P^{Eo} [MW]	P^{Ro} [MW]	$\mathcal{R}^E$ [€]	$\mathcal{R}^R$ [€]	$\tilde{r}$ [%]	$\tilde{\mathcal{R}}^E$ [€]	$\tilde{\mathcal{R}}^R$ [€]	$\overline{\Delta\mathcal{R}}$ [%]	$\overline{\Delta r}$ [%]
C_o	0	Classic	0.54	1.42	27.84	49.79	10.22	28.83	49.18	0.49	10.22
		Proposed	**1.28**	**0.71**	**51.87**	**24.89**	**0.00**	**51.77**	**24.89**	**-0.13**	**0.00**
	20	Classic	0.13	1.96	13.94	64.34	35.84	15.31	63.26	0.37	15.84
		Proposed	**0.46**	**1.65**	**22.88**	**55.54**	**19.71**	**22.70**	**55.62**	**-0.13**	**-0.29**
	40	Classic	0.00	2.09	11.51	66.82	43.91	12.77	65.75	0.24	3.91
		Proposed	**0.14**	**2.02**	**14.35**	**64.31**	**39.54**	**14.12**	**64.45**	**-0.11**	**0.01**
C_4	0	Classic	0.54	1.42	27.84	49.79	35.15	40.95	40.71	5.19	35.15
		Proposed	**2.33**	**0.00**	**81.30**	**0.00**	**0.00**	**80.95**	**0.00**	**-0.43**	**0.00**
	20	Classic	0.13	1.96	13.94	64.34	47.89	30.43	50.54	3.44	27.89
		Proposed	**1.55**	**0.88**	**54.91**	**27.70**	**19.64**	**54.56**	**27.66**	**-0.47**	**-0.36**
	40	Classic	0.00	2.09	11.51	66.82	50.18	28.10	52.55	2.96	10.18
		Proposed	**1.26**	**1.27**	**45.37**	**37.39**	**31.05**	**44.96**	**37.42**	**-0.46**	**-0.40**

The Bidding Behavior of WPP with the Non-Binding Reserve Unavailability Risk Constraint Can Be Interpreted By Noticing the Values Indicated By Underline.

Therefore, when comparing the performance of these approaches, one should be careful to look at classification accuracy and similarity metrics together. Interestingly, it is seen that by leveraging an auxiliary classifier, the classification performance of ACWGAN is significantly improved for all class labels compared to CWGAN. In particular, as shown in Fig. 3, the accuracy of ACWGAN for class labels C_o, C_1, C_2, C_3, and C_4, is significantly higher than that of CWGAN by 0.8%, 27.4%, 30.5%, 24.3%, and 8.2%, respectively.

C. Advantages of the Proposed WPP Scheduling Model

The obtained results of the classic and proposed WPP energy and reserve scheduling frameworks are summarized in Table III. The WPP's bidding performance with respect to three reserve market participation requirements, $\rho^o = \{0, 20, 40\}\%$, defined by TSO, for both classic and proposed frameworks is detailed. The comparative results are presented for very low, C_o, and high, C_4, wind fluctuation levels in Table III. The in-sample results, including the submitted energy bid P^{Eo} and reserve bid P^{Ro} to the market as well as the expected revenues from energy $\mathcal{R}^E$ and reserve $\mathcal{R}^R$, are provided in Table III. Moreover, the out-of-sample results regarding the real-time risk of reserve unavailability $\tilde{r}$, and revenues from energy $\tilde{\mathcal{R}}^E$ and reserve $\tilde{\mathcal{R}}^R$ are shown in Table III. The last column details the normalized total profit deviation, and risk of reserve unavailability deviation, which are calculated, respectively, by (21) and (22):

$$\overline{\Delta\mathcal{R}}\% = \frac{\left(\tilde{\mathcal{R}}^E + \tilde{\mathcal{R}}^R\right) - \left(\mathcal{R}^E + \mathcal{R}^R\right)}{\left(\mathcal{R}^E + \mathcal{R}^R\right)} \times 100\% \quad (21)$$

$$\overline{\Delta r}\% = \tilde{r} - r \quad (22)$$

where r is the expected risk of reserve unavailability and dropped from Table III for the sake of brevity. However, in the case of the experiment with the proposed framework on $\rho^o = 40\%$, the expected risk r is 39.53% and 31.45% regarding C_o and C_4,

respectively. It means that the WPP takes a risk lower than the reserve market participation requirement, ρ^{o}, in order to avoid the negative penalties associated with reserve unavailability. For the other experiments, the values of *r* and ρ^{o} are identical.

As seen in Table III, the in-sample results of the classic bidding model are invariable regarding the wind deviation levels, i.e., C_o and C_4. Its reason is that the classic model merely receives hourly wind uncertainty as input. However, the decisions are different concerning ρ^{o}. On the other hand, the proposed bidding framework returns different and relevant decisions based on both the wind deviation level and reserve market participation requirement ρ^{o}. For both models, as ρ^{o} increases, a higher bid is submitted to the reserve market floor, whereas a lower bid is devoted to the energy market floor. That arises from the fact that the incentives for reserve procurement are more encouraging for the WPP in the presented market setting (see Table I).

Interestingly, it can be observed that $\overline{\Delta r}\%$ for the proposed framework is very small, i.e., its out-of-sample risk result is close to the expected risk level. On the other hand, the classic method fails to stay reasonably close to the expected risk level. In particular, the maximum risk deviation for the proposed method is -0.4%, whereas for the classic method is 35.15%. The same pattern applies to real-time profit deviation $\overline{\Delta \mathcal{R}}\%$ as shown in Table III. Thus, the proposed method not only obtains higher total profit than the classic method, but also has significantly higher robustness, against wind power variations, compared with the classic method.

Nevertheless, in some cases, the total profits obtained with both methods are close (see Table III). However, this profit is not feasible for WPP using the classic method. The reason is that the corresponding scheduled bids obtained with classic method lead ex-post to a violation of the market participation requirement. For example, using the proposed bidding framework, with an ex-post profit of 80.95 €, the WPP does not bid any power quantity to the reserve market while the ultra-short-term wind fluctuations are too high, C_4, and ρ^{o} is zero. In contrast, with a slightly higher profit of 81.66 €, the classic model, by neglecting the ultra-short-term wind fluctuations, submits a rather high-power bid, $P^{Ro} = 1.42$ MW, to the reserve market floor. Accordingly, while Δr for the proposed method is zero, the classic model is unable to maintain the real-time reserve reliability leading to $\overline{\Delta r} = 35.15\%$. This violation may result in exclusion or suspension of participation in the reserve market.

Furthermore, the sensitivities of $\overline{\Delta r}$ and $\overline{\Delta R}$ to changes in wind deviations are much higher in the classic method than in the proposed method. It can be seen that for ρ^{o}= {0, 20, 40}%, in the classic method, $\overline{\Delta r}$ is higher for C_4, by {24.93, 12.05, 6.27}%, than for C_o. For instance, in the classic method, 24.93% is obtained by subtracting $\overline{\Delta r}$ of C_4 from $\overline{\Delta r}$ of C_o, where ρ^{o}= 0, i.e., 24.93 = 35.15-10.22. The other results in this paragraph are also obtained in a similar way. On the other hand, the corresponding deviations in $\overline{\Delta r}$ for the proposed method are only -{0.00, 0.07, 0.41}%. Moreover, $\overline{\Delta R}$ increases by {4.7, 3.07, 2.72}%, regarding ρ^{o}= {0, 20, 40}%, for the classic method due to the changes of wind deviation level from C_o to C_4. On the other hand, the corresponding deviations of $\overline{\Delta R}$ in the proposed method are only -{0.3, 0.34, 0.35}%. The reason for the lower sensitivity of the proposed method compared to the classical method is that the proposed method implicitly considers wind deviation levels as input to the bidding model via the scenarios generated by ACWGAN.

Similarly, the WPP's bidding behavior with the non-binding reserve unavailability risk constraint in both models can be interpreted from Table III. When ρ^{o} is sufficiently high (40% in this study), (11) becomes non-binding. Thus, both models bid in such a way that the trade-off between the day-ahead revenue and the real-time penalty is profitable regardless of the confidence level of reserve availability. The values regarding the wind power bidding, with reserve unavailability risk constraint non-binding, are underlined in Table III. It is seen that when the wind deviation level is low, C_o, the classic model obtains the expected total profit of 78.33 €, corresponding to $\mathcal{R}^E + \mathcal{R}^R$, and 78.52 € for the out-of-sample analysis. Also, the proposed framework yields a slightly higher profit of 78.66 € and 78.57 € concerning the in- and out-of-sample analysis, respectively. In addition, for high wind fluctuation level, C_4, the advantage of using the proposed method is more significant. The classic method obtains 78.33 € and 80.65 € regarding the in- and out-of-sample analysis, whereas the proposed framework attains a higher profit of 82.76 € and 82.38 € for the in- and out-of-sample analysis, i.e., 2.1% higher in the ex-post analysis.

Remarkably, by removing the probabilistic constraint (11), the proposed framework loses the reserve provision confidence, which has the probability of 1-39.54% = 60.46% and 1-31.05% = 68.95% regarding C_o and C_4 classes, respectively. The classic model has lower reserve provision confidence levels of 1-43.91% = 56.09% and 1-50.18% = 49.82% regarding C_o and C_4, respectively, which are similarly lost when (11) is removed. In this case, in both models, the TSO is not aware of the probability of the real-time reserve unavailability. However, by requiring the WPPs to fulfill a confidence level regarding the offered capacity, the proposed framework is able to respect the reserve market participation requirement, as seen from $\tilde{r}$ results in Table III. On the other hand, the classic model does not have this capability as seen from its $\tilde{r}$ results in Table III.

Thus, adopting a metric regarding reserve unavailability in the proposed WPP multi-resolution probabilistic bidding framework enables the TSO to have reliable insight on the real-time wind power share in reserve provision.

Meanwhile, the proposed multi-resolution bidding framework solves, for an hourly period and a single risk threshold, between 0.07 to 3.94 seconds on a DELL hardware set with Intel Core i7 CPU 2.6 GHz and 16 GB of RAM. This is a low computation time on a simple hardware set.

D. Advantage of Exploiting ACWGAN Compared to Other Scenario Representation Models in WPP Bidding Framework

In this section, the superiority of employing ACWGAN in the proposed bidding framework, in comparison with other scenario representation methods, is illustrated. Reserve unavailability risk deviation $\overline{\Delta r}\%$ and normalized profit deviation $\overline{\Delta \mathcal{R}}\%$ are used as evaluation metrics and are illustrated in Fig. 4(a) and (b), respectively. The horizontal categorical axis shows 5 class

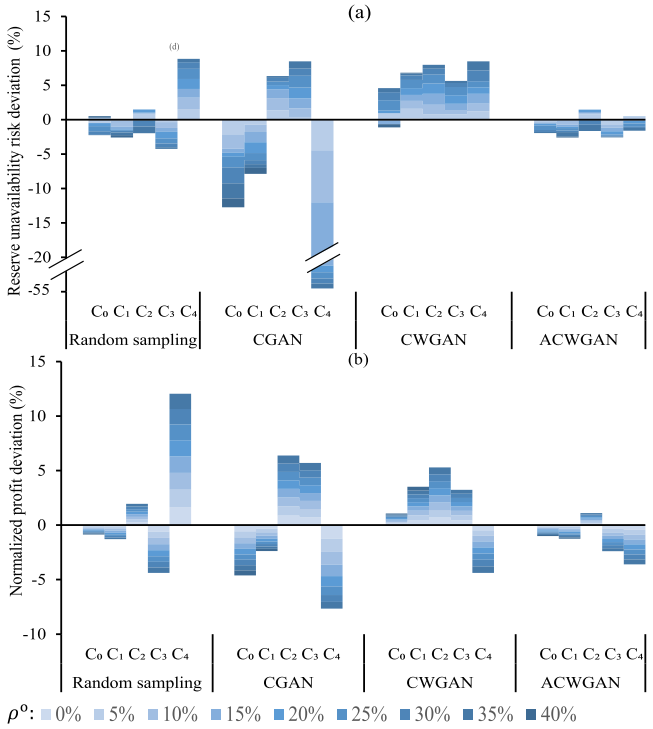

Fig. 4. Comparison of the proposed ACWGAN scenario generation method with direct sampling, CGAN, and CWGAN using the proposed WPP multi-resolution probabilistic bidding approach based on (a) reserve unavailability risk deviation metric and (b) normalized profit deviation metric.

labels regarding the wind mean deviation levels, C_o to C_4, and four scenario representation schemes.

The benchmark scenario representation methods presented for comparison with the proposed ACWGAN approach include direct random sampling from the training set, CGAN, and CWGAN. The vertical axis in Fig. 4(a) and (b) corresponds to $\overline{\Delta r}\%$ and $\overline{\Delta \mathcal{R}}\%$, respectively. Each bar segment within a stacked bar represents the value of the evaluation metric ($\overline{\Delta r}\%$ or $\overline{\Delta \mathcal{R}}\%$), regarding ρ°. It should be noted that a smaller magnitude of each stacked bar, regardless of its direction, corresponds to a better-performing approach. In this study, a fine resolution, i.e., 5%, concerning the reserve market participation requirement ρ° from 0 to 40% is considered.

As seen in Fig. 4(a), direct sampling from the training set obtains a lower deviation regarding reserve unavailability risk for all wind fluctuation levels, C_o to C_4, compared to CGAN. This observation can be explained considering that CGAN has a poor performance regarding the statistical and similarity metrics as well as classification accuracy.

Performance of the CWGAN regarding $\overline{\Delta r}\%$ is better than CGAN for all wind deviation levels while is nonetheless worse than the direct sampling method concerning C_o, C_1, C_2, and C_3. However, it can be seen that the CWGAN yields a lower deviation compared to the direct sampling approach for C_4 and almost a similar deviation concerning C_3. That is because these are less-probable classes in the training set. Thus, since enough samples are not available, direct sampling cannot provide a good approximation to represent the wind deviation uncertainty for these classes. Besides, CGAN does not perform well for the less-probable classes as it is known to suffer from mode collapse. Remarkably, ACWGAN scenario generation method is shown to outperform other GAN-based and direct sampling methods in terms of the deviations of the risk of reserve unavailability in all classes.

Regarding the normalized profit deviation, as shown in Fig. 4(b), direct sampling performs better than CGAN for wind deviation levels C_o to C_3. On the other hand, CWGAN performs better than CGAN for C_o, C_2, C_3, C_4 and is very close to CGAN in the case of C_1. Specifically, regarding less-probable classes, CWGAN performs significantly better than direct sampling and CGAN. Finally, ACWGAN outperforms direct sampling and the other GAN-based scenario generation schemes since the magnitude of its stacked bar corresponding to each class label is lower than the other alternatives.

V. Conclusion

Participation of wind power producers (WPPs) in the day-ahead energy and reserve market requires designing dedicated decision tools that consider the stochastic process of the wind at both low and high temporal resolutions. Accordingly, an efficient scenario generation tool based on auxiliary classifier Wasserstein GAN is firstly proposed to produce the wind mean deviation scenarios regarding the ultra-short-term wind uncertainty. The superiority of the proposed scenario generation technique over the conditional GAN and its Wasserstein-based counterpart using statistical and similarity metrics is illustrated. Then, a multi-resolution probabilistic WPP bidding framework, comprising a novel probabilistic constraint, regarding the reliability of the reserve bids, and the proposed ultra-short-term scenario generation approach, is devised. It is shown that compared to the outcomes of the single-resolution model, the profit loss and reserve reliability are significantly improved by the proposed data-driven WPP decision-making framework. Finally, the significance of the devised modules in the proposed framework is shown by comparing deviations from the expected revenue and reserve unavailability risk with the results obtained by other scenario representation alternatives. Future research could consider the impact of ultra-short-term wind variations in market prices for possible cases where wind power producers participate in the market as price-maker.

References

[1] L. Exizidis, J. Kazempour, A. Papakonstantinou, P. Pinson, Z. De Grève, and F. Vallée, "Incentive-compatibility in a two-stage stochastic electricity market with high wind power penetration," *IEEE Trans. Power Syst.*, vol. 34, no. 4, pp. 2846–2858, Jul. 2019.

[2] M. Shamsi and P. Cuffe, "A prediction market trading strategy to hedge financial risks of wind power producers in electricity markets," *IEEE Trans. Power Syst.*, vol. 36, no. 5, pp. 1–12, Sep. 2021.

[3] J. Bottieau, L. Hubert, Z. De Greve, F. Vallee, and J.-F. Toubeau, "Very-short-term probabilistic forecasting for a risk-aware participation in the single price imbalance settlement," *IEEE Trans. Power Syst.*, vol. 35, no. 2, pp. 1218–1230, Mar. 2020.

[4] J. Matevosyan and L. Soder, "Minimization of imbalance cost trading wind power on the short-term power market," *IEEE Trans. Power Syst.*, vol. 21, no. 3, pp. 1396–1404, Aug. 2006.

[5] A. Giannitrapani, S. Paoletti, A. Vicino, and D. Zarrilli, "Bidding wind energy exploiting wind speed forecasts," *IEEE Trans. Power Syst.*, vol. 31, no. 4, pp. 2647–2656, Jul. 2016.
[6] J. Bottieau, F. Vallée, Z. De Grève, and J.-F. Toubeau, "Leveraging provision of frequency regulation services from wind generation by improving day-ahead predictions using LSTM neural networks," in *Proc. IEEE Int. Energy Conf.*, Limassol, Cyprus, 2018, pp. 1–6.
[7] H. Li, Y. Qiao, Z. Lu, B. Zhang, and F. Teng, "Frequency constrained stochastic planning towards a high renewable target considering frequency response support from wind power," *IEEE Trans. Power Syst.*, vol. 36, no. 5, pp. 1–13, Sep. 2021.
[8] J. Liang, S. Grijalva, and R. Harley, "Increased wind revenue and system security by trading wind power in energy and regulation reserve markets," *IEEE Trans. Sustain. Energy*, vol. 2, no. 3, pp. 340–347, Jul. 2011.
[9] T. Soares, P. Pinson, T. Jensen, and H. Morais, "Optimal offering strategies for wind power in energy and primary reserve markets," *IEEE Trans. Sustain. Energy*, vol. 7, no. 3, pp. 1036–1045, Jul. 2016.
[10] T. Soares, T. Jensen, N. Mazzi, P. Pinson, and H. Morais, "Optimal offering and allocation policies for wind power in energy and reserve markets," *Wind Energy*, vol. 20, no. 11, pp. 1851–1870, 2017.
[11] S. A. Hosseini, J.-F. Toubeau, Z. De Grève, and F. Vallée, "An advanced day-ahead bidding strategy for wind power producers considering confidence level on the real-time reserve provision," *Appl. Energy,* vol. 280, 2020, Art. no. 115973.
[12] S. A. Hosseini *et al.*, "Impact of fast wind fluctuations on the profit of a wind power producer jointly trading in energy and reserve markets," in *Proc. 9th IET Int. Conf. Renewable Power Gen., RPG 2021*, Dublin, Ireland, 2021.
[13] Y. Chen, Y. Wang, D. Kirschen, and B. Zhang, "Model-free renewable scenario generation using generative adversarial networks," *IEEE Trans. Power Syst.*, vol. 33, no. 3, pp. 3265–3275, May 2018.
[14] X. Yang, H. He, J. Li, and Y. Zhang, "Toward optimal risk-averse configuration for HESS with CGANs-based PV scenario generation," *IEEE Trans. Syst. Man Cybern. Syst.*, vol. 51, no. 3, pp. 1–15, Mar. 2021.
[15] A. De Leon and K. Chough, *Analysis of Mixed Data: Methods & Applications*, 1st ed. Chapman and Hall/CRC, 2013.
[16] Z. Liang, X. Su, and K. Feng, "Drought propagation and construction of a comprehensive drought index based on the Soil and Water Assessment Tool (SWAT) and empirical Kendall distribution function (K C′: A case study for the Jinta River basin in northwestern China," *Nat. Hazards Earth Syst. Sci.*, vol. 21, no. 4, pp. 1323–1335, 2021.
[17] C. Jiang, Y. Mao, Y. Chai, M. Yu, and S. Tao, "Scenario generation for wind power using improved generative adversarial networks," *IEEE Access*, vol. 6, pp. 62193–62203, 2018.
[18] Y. Wang, G. Hug, Z. Liu, and N. Zhang, "Modeling load forecast uncertainty using generative adversarial networks," *Electr. Power Syst. Res.*, vol. 189, 2020, Art. no. 106732.
[19] C. Zhao, C. Chen, Z. He, and Z. Wu, "Application of auxiliary classifier wasserstein generative adversarial networks in wireless signal classification of illegal unmanned aerial vehicles," *Appl. Sci.*, vol. 8, no. 12, 2018, Art. no. 26-64.
[20] C. Zhao, C. Chen, Z. Cai, M. Shi, X. Du, and M. Guizani, "Classification of small UAVs based on auxiliary classifier wasserstein GANs," in *Proc. IEEE GLOBECOM*, Abu Dhabi, UAE, 2018, pp. 206–212.
[21] M. Lydia, A. I. Selvakumar, S. S. Kumar, and G. E. P. Kumar, "Advanced algorithms for wind turbine power curve modeling," *IEEE Trans. Sustain. Energy,* vol. 4, no. 3, pp. 827–835, Jul. 2013.
[22] V. Thapar, G. Agnihotri, and V. Sethi, "Critical analysis of methods for mathematical modelling of wind turbines," *Renew. Energy*, vol. 36, no. 11, pp. 3166–3177, 2011.
[23] S. Shokrzadeh, M. Jafari Jozani, and E. Bibeau, "Wind turbine power curve modeling using advanced parametric and nonparametric methods," *IEEE Trans. Sustain. Energy*, vol. 5, no. 4, pp. 1262–1269, Oct. 2014.
[24] Nordic Balancing Model, "Current requirements for production plans and imbalances, monitoring and the use of production plans in balancing," *Nordic Balancing Model*, 2020. Accessed: Mar. 8, 2022. [Online]. Available: https://nordicbalancingmodel.net/wp-content/uploads/2020/03/Current-requirements-for-production-plans-and-imbalances_FINAL.pdf
[25] K. Van den Bergh and E. Delarue, "Energy and reserve markets: Interdependency in electricity systems with a high share of renewables," *Electr. Power Syst. Res.*, vol. 189, 2020, Art. no. 106537.
[26] J. -F. Toubeau, J. Bottieau, Z. De Grève, F. Vallée, and K. Bruninx, "Data-driven scheduling of energy storage in day-ahead energy and reserve markets with probabilistic guarantees on real-time delivery," *IEEE Trans. Power Syst.*, vol. 36, no. 4, pp. 2815–2828, Jul. 2021.
[27] Elia, "Public consultation on Terms and Conditions for balancing service providers for automatic Frequency Restoration Reserve (aFRR)," Elia, 2020. Accessed: Mar. 08, 2020. [Online]. Available: https://www.elia.be/-/media/project/elia/elia-site/public-consultations/2020/20200303_consultationreport_tc_bsp-afrr---final---non-confidential_en.pdf
[28] I. Durbach and T. Stewart, "Using expected values to simplify decision making under uncertainty," *Omega*, vol. 37, no. 2, pp. 312–330, 2009.
[29] C. Potter and M. Negnevitsky, "Very short-term wind forecasting for Tasmanian power generation," *IEEE Trans. Power Syst.*, vol. 21, no. 2, pp. 965–972, May 2006.
[30] M. Hossain, R. Chakrabortty, S. Elsawah, and M. Ryan, "Very short-term forecasting of wind power generation using hybrid deep learning model," *J. Clean. Prod.*, vol. 296, 2021, Art. no. 126564.
[31] J. Wang, M. Shahidehpour, and Z. Li, "Security-constrained unit commitment with volatile wind power generation," *IEEE Trans. Power Syst.*, vol. 23, no. 3, pp. 1319–1327, Aug. 2008.
[32] P. Pinson, H. Madsen, H. Nielsen, G. Papaefthymiou, and B. Klöckl, "From probabilistic forecasts to statistical scenarios of short-term wind power production," *Wind Energy*, vol. 12, no. 1, pp. 51–62, 2009.
[33] S. Albatran, S. Harasis, M. Ialomoush, Y. Alsmadi, and M. Awawdeh, "Realistic optimal power flow of a wind-connected power system with enhanced wind speed model," *IEEE Access*, vol. 8, pp. 176973–176985, 2020.
[34] S. Rahmani and N. Amjady, "A new optimal power flow approach for wind energy integrated power systems," *Energy*, vol. 134, pp. 349–359, 2017.
[35] M. Padala, D. Das, and S. Gujar, "Effect of input noise dimension in GANs," *Lecture Notes Comput. Sci. (LNCS)*, vol. 13110, pp. 558–569, 2021, doi: 10.1007/978-3-030-92238-2_46.
[36] M. Arjovsky, S. Chintala, and L. Bottou, "Wasserstein generative adversarial networks," in *Proc. 34th Int. Conf. Mach. Learn. (PMLR)*, Sydney, Australia, vol. 70, 2017.
[37] B. Adlam, C. Weill, and A. Kapoor, "Investigating under and overfitting in wasserstein generative adversarial networks," in *ICML Understanding Improving Generalization Deep Learn. Workshop*, 2019, *arXiv:1910.14137v1*.
[38] I. Gulrajani, F. Ahmed, M. Arjovsky, V. Dumoulin, and A. Courville, "Improved training of Wasserstein GANs," in *Adv. Neural Inf. Process. Syst. (NIPS)*, California, USA, 2017, *arXiv:1803.01541*.
[39] Y. Zhang and Q. Yang, "A survey on multi-task learning," *IEEE Trans. Knowl. Data Eng.*, to be published, doi: 10.1109/TKDE.2021.3070203.
[40] "D3.2 definition of new/changing requirements for market designs," interrface.eu, 2020. Accessed: Sep. 1, 2021. [Online]. Available: http://www.interrface.eu/sites/default/files/publications/INTERRFACE_D3.2_v1.0.pdf
[41] "Frequency containment reserves (FCR)," entsoe.eu, 2021. Accessed: Sep. 1, 2021. [Online]. Available: https://www.entsoe.eu/network_codes/eb/fcr/
[42] "Datasets," *Energinet*, 2021. Accessed: Aug. 16, 2021. [Online]. Available: https://www.energidataservice.dk/search
[43] "ENTSO-E Transparency Platform," *Transparency.entsoe.eu*, 2021. [Online]. Available: Accessed: Aug. 16, 2021. [Online]. Available: https://transparency.entsoe.eu/
[44] P. Domagalski and L. R. Sætran, "Frøya wind data (1Hz)," 2019, doi: 10.5281/ZENODO.3403362.
[45] M. Fekri, A. Ghosh, and K. Grolinger, "Generating energy data for machine learning with recurrent generative adversarial networks," *Energies*, vol. 13, no. 1, 2019, Art. no. 130.
[46] F. Ye, F. Zhu, Y. Fu, and B. Shen, "ECG generation with sequence generative adversarial nets optimized by policy gradient," *IEEE Access*, vol. 7, pp. 159369–159378, 2019.

Seyyed Ahmad Hosseini (Student Member, IEEE) received the B.S. degree in electrical engineering from Rajaee University, Tehran, Iran, in 2011, and the M.S. degree in electrical engineering from Semnan University, Semnan, Iran, in 2014. He is currently working toward the Ph.D. degree with the Power Systems and Markets Research Group, University of Mons, Mons, Belgium. He was a Visiting Lecturer with Iran Technical and Vocational University. His research interests include machine learning, integration of wind power in electricity markets, decision-making under uncertainty, and power system stability.

Jean-François Toubeau (Member, IEEE) received the master's and Ph.D. degrees in electrical engineering from the University of Mons, Mons, Belgium, in 2013 and 2018, respectively. He is currently a Postdoctoral Researcher with the Belgian Fund for Research (F.R.S/FNRS), Power Systems and Markets Research Group, University of Mons. Since July 2021, he has been a Visiting Researcher with Imperial College London, London, U.K. His research interests include machine learning and decision-making in modern power systems.

Zacharie De Grève (Member, IEEE) received the Electrical and Electronics Engineering degree from the Faculty of Engineering, University of Mons, Mons, Belgium, in 2007, and the Ph.D. degree in electrical engineering from the University of Mons, in 2012. He was a Research Fellow of the Belgian Fund for Research (F.R.S/FNRS) till 2012. He is currently an Associate Professor with the Electrical Power Engineering Unit, University of Mons. His main research interests include the application of machine learning and operations research to electric power systems, and energy systems more generally. He also develops expertise in computational electromagnetics.

Yi Wang (Member, IEEE) received the B.Sc. degree from the Huazhong University of Science and Technology, Wuhan, China, in June 2014, and the Ph.D. degree from Tsinghua University, Beijing, China, in January 2019. From March 2017 to April 2018, he was a Visiting Student with the University of Washington, Seattle, WA, USA. From February 2019 to August 2021, he was a Postdoctoral Researcher with Power Systems Laboratory, ETH Zurich, Zürich, Switzerland. He is currently an Assistant Professor with the Department of Electrical and Electronic Engineering, The University of Hong Kong, Hong Kong. His research interests include data analytics in smart grids, energy forecasting, multienergy systems, Internet of Things, and cyber-physical-social energy systems.

Nima Amjady (Senior Member, IEEE) received the B.Sc., M.Sc., and Ph.D. degrees in electrical engineering from the Sharif University of Technology, Tehran, Iran, in 1992, 1994, and 1997, respectively. He is currently a Full Professor with the Department of Electrical Engineering, Semnan University, Semnan, Iran. He is also the Consultant of Semnan University President. In 2007, he was selected as an Iran's youngest Professor. He collaborates as a Consultant with electric power companies in Iran. His research interests include forecast processes and operation and planning of power systems.

François Vallée (Member, IEEE) received the degree in civil electrical engineering and the Ph.D. degree in electrical engineering from the Faculty of Engineering, University of Mons, Mons, Belgium, in 2003 and 2009, respectively. He is currently a Professor and the Leader with the Power Systems and Markets Research Group, University of Mons. His research interests include PV and wind generation modeling for electrical system reliability studies in presence of dispersed generation. His Ph.D. work has been awarded by the SRBE/KBVE Robert Sinave Award in 2010.